# Morphodynamic controls on redox conditions and on nitrogen dynamics within the hyporheic zone: Application to gravel bed rivers with alternate-bar morphology

A. Marzadri,[1] D. Tonina,[1] and A. Bellin[2]

Received 30 January 2012; revised 27 July 2012; accepted 1 August 2012; published 20 September 2012.

[1] Hyporheic flows, which stem from the interaction between stream flow and bedform, transport solute-laden surface waters into the streambed sediments, where reactive solutes undergo biogeochemical transformations. Despite the importance of hyporheic exchange on riverine ecosystem and biogeochemical cycles, research is limited on the effects of hyporheic fluxes on the fate of reactive solutes within the hyporheic zone. Consequently, we investigate the controls of hyporheic flowpaths, which we link to stream morphology and streamflow, on prevailing hyporheic redox conditions and on biogeochemical transformations occurring within streambeds. We focus on the dissolved inorganic reactive forms of nitrogen, ammonium and nitrate, because nitrogen is one of the most common reactive solutes and an essential nutrient found in stream waters. Our objectives are to explore the influence of stream morphology, hyporheic water temperature and relative abundance of ammonium and nitrate, on transformation of ammonium, removal of nitrates and production of nitrous oxide, a potent greenhouse gas. We address our objectives with analytical solutions of the Multispecies Reactive Advection-Dispersion Equation coupled with linearized Monod's kinetics and analytical solutions of the hyporheic flow for alternate-bar morphology. We introduce a new Damköhler number, *Da*, defined as the ratio between the median hyporheic residence time and the time scale of oxygen consumption, which we prove to be a good indicator of where aerobic or anaerobic conditions prevail. In addition, *Da* is a key index to quantify hyporheic nitrification and denitrification efficiencies and defines a new theoretical framework for scaling results at both the morphological-unit and stream-reach scales.

**Citation:** Marzadri, A., D. Tonina, and A. Bellin (2012), Morphodynamic controls on redox conditions and on nitrogen dynamics within the hyporheic zone: Application to gravel bed rivers with alternate-bar morphology, *J. Geophys. Res.*, *117*, G00N10, doi:10.1029/2012JG001966.

## 1. Introduction

[2] Dissolved inorganic reactive nitrogen (Nr) is a common solute found in stream waters. It affects water quality, plant growth, aquatic and terrestrial ecosystems, but is also one of the main cause of eutrophication of water bodies [*Spalding and Exner*, 1993; *Galloway et al.*, 2003]. Nr is present at low concentrations in natural stream waters, but many streams flowing in agricultural and urban areas suffer from an excess of Nr, typically in the form of ammonium ($NH_4^+$) and nitrate ($NO_3^-$) [*Alexander et al.*, 2000; *Peterson et al.*, 2001]. Microbial processes are the primary mechanisms reducing nitrogen loads by removing Nr species from rivers [*Master et al.*, 2005]. Under oxidizing conditions, aerobic bacteria use dissolved oxygen (DO) as a terminal acceptor to transform ammonium into nitrate (nitrification), whereas under reducing conditions, in the presence of electron donor compounds such as organic carbon, anaerobic bacteria reduce nitrate to nitrous oxide ($N_2O$) and/or molecular nitrogen ($N_2$) through denitrification [e.g., *Naiman and Bilby*, 1998]. These transformations occur primarily in the streambed sediment, where the rich microbial community colonizing the streambed particle surfaces are in contact with solutes dissolved in the stream water [*Master et al.*, 2005]. In fact, hyporheic exchange is the primary mechanism that delivers stream solutes within the streambed sediment and mixes solute-laden waters between stream and pore waters [e.g., *Tonina and Buffington*, 2009a, and citations therein].

[3] Field investigations of nitrogen cycle support the importance of hyporheic exchange in nutrient cycling in

[1]Center for Ecohydraulics Research, University of Idaho, Boise, Idaho, USA.
[2]Department of Civil and Environmental Engineering, University of Trento, Trento, Italy.

Corresponding author: A. Marzadri, University of Idaho, Center for Ecohydraulics Research, 322 E. Front St., Ste. 340, Boise, ID 83702, USA. (amarzadri@uidaho.edu)

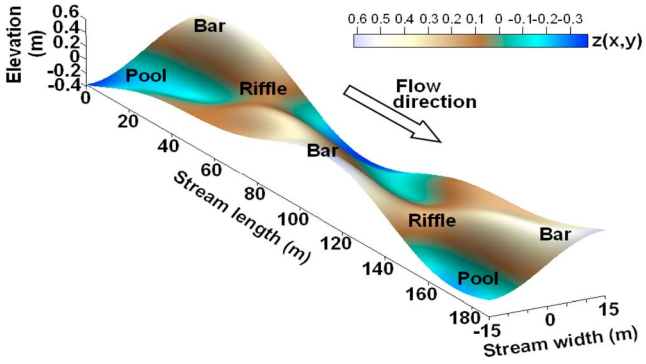


**Figure 1.** Reach with alternate-bar topography ($z$). The coordinates $x$, $y$, and $z$ are positive downstream, leftward, and upward.

rivers [*Alexander et al.*, 2000; *Binley*, 2005] and of the hyporheic zone (HZ) as a transformation hot spot, zone with high biogeochemical transformation, for nitrogen compounds [*Triska et al.*, 1993; *Mulholland et al.*, 2004; *Zarnetske et al.*, 2011]. Additionally, numerical simulations of hyporheic chemistry within dunes at the sea floor [*Cardenas et al.*, 2008] and within stream meanders [*Boano et al.*, 2010] show the importance of hyporheic flow structure in biogeochemical zonation of the hyporheic zone.

[4] Despite these evidences, there is a lack of knowledge on the controls of streambed morphology, which is a primary driver of hyporheic flows [e.g., *Tonina and Buffington*, 2009a], on hyporheic biogeochemical processes. In the present work, we investigate the control of stream morphology and flow on prevailing aerobic and anaerobic conditions within the streambed hyporheic zone. In addition, we quantify the efficiency of the hyporheic zone in transforming ammonium, removing nitrates and in producing nitrous oxide as a function of stream morphology and ambient conditions, such as hyporheic water temperature and relative abundance of ammonium and nitrate. We show that prevailing redox conditions within the hyporheic zone can be predicted according to the value assumed by a new dimensionless number, *Da*, defined as the ratio between the hyporheic median residence time and the time of consuming dissolved oxygen to a prescribed threshold concentration below which reducing reactions are activated.

[5] To address our objectives, we use a Lagrangian model based on analytical solutions of the Multi Species Reactive Advection-Dispersion Equation (RADE) with advection obtained by solving the flow equation within the hyporheic zone, and expressing Nr transformations as a function of the travel time distribution of a passive solute. This model is a generalization of the semi-analytical model proposed by *Marzadri et al.* [2011] in the absence of dispersion. Here, we focus on alternate-bar morphology because of its ecological importance and ubiquity in gravel bed rivers [*Tonina and Buffington*, 2007; *Buffington and Tonina*, 2009]. This bed form is composed of an alternate sequence of pools, where water is deep and slow, and riffles, where flow is shallow and fast, with two successive diagonal fronts delimiting the bar unit with a pool at the downstream end of each front in proximity of the channel banks (Figure 1) [e.g., *Tonina and Buffington*, 2009b].

## 2. Method

### 2.1. Hyporheic Flow

[6] We consider a straight gravel bed river of constant width and discharge with alternate-bar morphology and a homogeneous and isotropic hydraulic conductivity ($K$) of the streambed sediment. Under these hypotheses, the governing equation of the hydraulic head $h$ assumes the following form [*Marzadri et al.*, 2010]:

$$\frac{\partial^2 h}{\partial x^2}+\frac{\partial^2 h}{\partial y^2}+\frac{\partial^2 h}{\partial z^2}=0, \tag{1}$$

which can be solved analytically with the following boundary conditions (see Figure 1):

$$\begin{cases} \dfrac{\partial h}{\partial y}=0 & for \quad y=(+B,-B) \\ h\left(-\dfrac{L}{2},y,z\right)=h\left(\dfrac{L}{2},y,z\right) & \\ \dfrac{\partial h}{\partial z}=0 & for \quad z=-z_d \\ h(x,y,0)=h_b(x,y) & \end{cases}, \tag{2}$$

where $x$, $y$ and $z$ are the spatial coordinates, $2B$ is the channel width, $Y_0$ is the mean flow depth above the mean streambed elevation, which is fixed at z = 0, $z_d$ is the alluvium depth, $L$ is bar wavelength and $h_b$ is the head at the stream bed. In the present work, we approximate $h_b$ with the theoretical expression provided by *Colombini et al.* [1987], but other approximations, analytical, numerical or empirical, may be used when needed [e.g., *Elliott and Brooks*, 1997; *Marion et al.*, 2002; *Tonina and Buffington*, 2009b, 2011]. Strictly speaking, this condition should be applied to the surface $z = \eta(x, y)$, representing the elevation of the streambed above its mean (Figure 1). However, in a previous paper [*Marzadri et al.*, 2010] we showed that applying it to the plane $z = 0$ modifies only slightly the distribution of $h$ with negligible effects on the travel time distribution within the hyporheic zone. This assumption dramatically simplifies the differential equation and allows deriving an analytical solution for the head.

[7] Once $h$ is known from the solution of equation (1) with the boundary conditions (2), it can be substituted into the Darcy equation:

$$\mathbf{u}=-\frac{K}{\vartheta}\nabla h \tag{3}$$

to obtain the velocity field $\mathbf{u}[u, v, w]$. In equation (3) $\vartheta$ is the alluvium porosity, such that the hyporheic flux is $\mathbf{q} = \vartheta\ \mathbf{u}$.

[8] In the present work, we employ the analytical solutions of the equations (1) and (3) with the boundary conditions (2) obtained by [*Marzadri et al.*, 2010].

### 2.2. Biogeochemical Model

[9] We model the nitrogen cycle within the hyporheic zone by using the simplified conceptual model depicted in Figure 2, which accounts for nitrification, denitrification, and biomass uptake [*Valett et al.*, 1996; *Pinay et al.*, 2009;

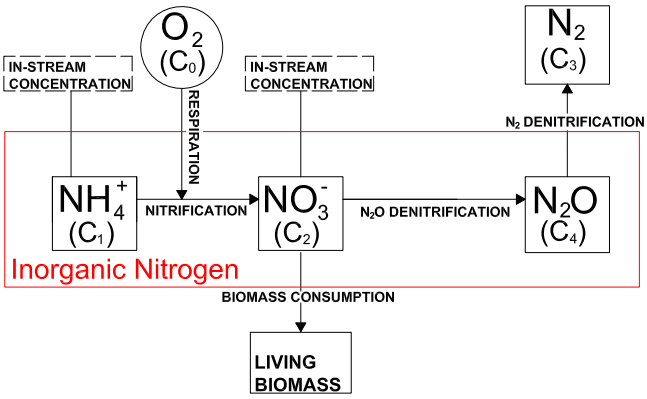


**Figure 2.** Proposed nitrogen cycle within the hyporheic zone.

*Zarnetske et al.*, 2011]. Nitrogen transformations are controlled by the reaction rates $f_i$ of dissolved oxygen ($i = 0$), and the four nitrogen species ($i$ = 1,2,3 and 4 for ammonium, nitrate, dinitrogen and nitrous oxide, respectively) reported in the Appendix A (equations (A5)–(A7)). As discussed by *Marzadri et al.* [2011], these linear reaction rates are obtained from linearization of the Monod's kinetics and are shown to provide a very good approximation of nitrogen transformations in both natural and biogeochemically altered rivers, where the concentrations of Nr species are typically much smaller than the corresponding equilibrium concentrations in the Monod's equations [*Buss et al.*, 2006; *Kjellin et al.*, 2007].

[10] Besides the concentration of the nitrogen species, other important factors control biological activity, such as dissolved oxygen ($C_0$), organic carbon, pH and water temperature. Dissolved oxygen concentrations are about 9–10 mg/l (at the water temperature of 15°C) in well aerated streams, but conditions shift from aerobic to anaerobic when $C_0$ falls below a given threshold $C_{0,\mathrm{lim}}$. In line with our simplified geochemical model, we assume that aerobic reactions (nitrification and biomass respiration), which consume oxygen, are active along the flow paths where $C_0 > C_{0,\mathrm{lim}}$. However, from where this limit is reached inward, redox conditions are not longer favorable to nitrification, which ceases, while denitrification is triggered [*Böhlke and Denver*, 1995].

[11] Nutrient cycling is also influenced by the ratio between ammonium and nitrate concentrations in streams [*Sjodin et al.*, 1997], because ammonium is a source of nitrate through nitrification. We identify the relative abundance of one with respect to the other Nr species through the following coefficient:

$$RC = \frac{C_{1,0}}{C_{2,0}}, \tag{4}$$

where the subscript 0 indicates the concentrations at the entry downwelling surface. Therefore $RC < 1$ identifies stream with relative abundance of nitrate with respect to ammonium. As in the work of [*Marzadri et al.*, 2011], we neglect the Dissimilatory Nitrate Reduction to Ammonium (DNRA), which has been recently observed in soils [*Sylvia et al.*, 2005], but it is considered a minor factor in streambed [*Kelso et al.*, 1999; *Puckett et al.*, 2008; *Duff and Triska*, 2000]. Furthermore, we neglect the ANAMMOX reaction occurring during the anaerobic oxidation of $NH_4^+$ to $N_2O$ because very little is known regarding its relevance with respect to aerobic nitrification in surface and subsurface water bodies [*Kendall et al.*, 2007].

[12] Finally, we assume that organic carbon (C) is not a limiting factor and that pH is constant. With the former assumption, we implicitly consider that the molar ratio between C:N is within the range from 30 to 40, for which mineralization and immobilization reactions are balanced [*Maier et al.*, 2009], a common condition in most real streams [*Arango and Tank*, 2008]. With the latter assumption, we neglect the effect of pH variations on redox conditions. Finally, we account for the temperature effects on the reaction rates through the Arrhenius equation [*Fogler*, 1999]:

$$K_{i(T)} = K_{i(20^\circ C)} \varphi_i^{T-20^\circ C}, \tag{5}$$

where $K_i$ are the rate coefficients at the hyporheic temperature $T$, which for simplicity is assumed constant within the hyporheic zone, $K_{i(20^\circ\mathrm{C})}$ are the rate coefficients at 20°C and $\varphi_i$ are the temperature coefficients (dimensionless).

### 2.3. Solute Transport Model

[13] The total mass flux $Q_M^i$ of the $i$-th species across the upwelling surface can be written as the summation of the contributions from the streamlines crossing the surface, as follows [*Marzadri et al.*, 2011]:

$$\begin{aligned} Q^i_{M,up}(t) &= \int_{A_{uw}} q(\boldsymbol{\xi})\ C_{f,i}\left[\tau_{up}(\mathbf{a}), t\right]\ dA(\boldsymbol{\xi}) \\ &= \int_{A_{dw}} q(\mathbf{a})\ C_{f,i}\left[\tau_{up}(\mathbf{a}), t\right]\ dA(\mathbf{a}), \quad i = 0, \ldots, 4, \end{aligned} \tag{6}$$

where $q(\mathbf{a})$ is the component of the downwelling flux normal to the infinitesimal cross section area $dA(\mathbf{a})$ of the streamline originating from $\mathbf{x} = \mathbf{a}$ within the downwelling surface $A_{dw}$. The corresponding quantities at the upwelling surface are $q(\boldsymbol{\xi})$ and $dA(\boldsymbol{\xi})$, respectively, with $\boldsymbol{\xi}$ indicating the position where the same streamline crosses the upwelling surface. The second right-hand expression in equation (6) is obtained by imposing the continuity equation along the streamline: $q(\mathbf{a})dA(\mathbf{a}) = q(\boldsymbol{\xi})\ dA(\boldsymbol{\xi})$. The travel time $\tau$ assumes the following expression [*Shapiro and Cvetkovic*, 1988; *Dagan et al.*, 1992; *Cvetkovic and Dagan*, 1994]:

$$\tau(\mathbf{a}) = \int_0^{s(\mathbf{a})} \frac{ds'}{u(s')}, \tag{7}$$

where $s'$ is the distance from $\mathbf{a}$ measured along the streamline, $u(s')$ is the velocity at the same position and $s(\mathbf{a})$ is the distance from the origin of the point where the travel time is evaluated. Notice that at each travel time $\tau(\mathbf{a})$ is associated a position $s(\mathbf{a})$ along the streamline. The dependence from $\mathbf{a}$ is introduced to identify the streamline. Hereafter, we indicate with $\tau_{up}(\mathbf{a})$ the time needed by the particle entering the hyporheic zone at $\mathbf{x} = \mathbf{a}$ to reach the upwelling surface at the position $\mathbf{x} = \boldsymbol{\xi}$. Notice that at each position $\boldsymbol{\xi}$ within the upwelling area corresponds a single value of $\tau_{up}$. Consequently, the probability distribution of $\tau_{up}(\mathbf{a})$ describes the hyporheic residence time distribution of stream waters within the alluvial sediments. In the following, for simplicity of notation, we omit the dependance of $\tau$ from $\mathbf{a}$.

[14] The concentration flux of the $i$-th species at the position where the streamline crosses the upwelling surface is defined as follows:

$$C_{f,i}[\tau_{up}, t] = C_i[\tau_{up}, t] - \frac{D_L \vartheta^2}{q(\xi)^2} \frac{\partial C_i}{\partial \tau}\Big|_{\tau=\tau_{up}}, \quad (8)$$

where $D_L = D_L + \alpha_L q(\boldsymbol{\xi})/\vartheta$ is the effective longitudinal dispersion coefficient. In equation (8) $D_M$ is the molecular diffusion and $\alpha_L$ is the longitudinal local dispersivity, which is assumed constant through the domain, such that the longitudinal component of the mechanical dispersion tensor depends linearly from the local velocity. Classical experimental results summarized by *Saffman* [1960] and *Pfankuch* [1963] and later reinterpreted by *Bear* [1972] suggest that for grain Peclet numbers, $Pe = q\, d_{50}/(\vartheta\, D_M)$, larger than 100, the experimental longitudinal dispersivity is well approximated by the following expression: $\alpha_L = \beta_B\, d_{50}$, where $d_{50}$ is the median grain size of the sediment and $\beta_B \simeq 1.8$. In the present work, we assumed $d_{50} = 0.01$ m, which leads to $\alpha_L = 0.018$ m.

[15] An expression similar to equation (6) can be written for any other surface crossed by the streamlines including the downwelling area:

$$Q^i_{M,dw}(t) = \int_{A_{dw}} q(\mathbf{a})\ C_{f,i}(0,t) dA(\mathbf{a}), \quad (9)$$

where $C_{f,i}(0, t)$ is the concentration of the species $i$ in the stream water. The concentration flux $C_{f,i}$, $i = 0, 1, 2, 3, 4$ of dissolved oxygen and the four Nr species is obtained by substituting into equation (8) the expressions of the resident concentrations obtained by solving the RADE along the streamlines with reaction rates provided in the Appendix A and neglecting lateral local dispersion:

$$\frac{\partial}{\partial \tau} C_i(\tau, t) + \frac{\partial}{\partial t} C_i(\tau, t) = \frac{D_L \vartheta^2}{q(s)^2} \frac{\partial^2}{\partial \tau^2} C_i(\tau, t) + f_i, \quad i = 0, 1, 2, 3. \quad (10)$$

[16] Solutions of the equation (10), with the biogeochemical model reported in Appendix A, are provided in Appendix B, which for completeness also reports the solution developed by *Marzadri et al.* [2011] for purely advective transport, i.e., by assuming $D_L = 0$ in equation (10). Similar solutions, but for a different biogeochemical model, have been obtained by *van Genuchten and Alves* [1982] and *Gelhar and Collins* [1971], while *Bellin and Rubin* [2004] adopted a similar approach to solve the ADE for a non-reactive tracer. Solutions provided in Appendix B are with the concentration of the Nr species normalized with respect to the total downwelling dissolved inorganic reactive nitrogen concentration: $Nr_0 = C_{1,0} + C_{2,0}$.

[17] Nitrification processes and respiration of the biomass consume oxygen within the hyporheic zone, such that aerobic processes are active from the downwelling area (which is identified by $\tau = 0$ in our Lagrangian reference system), where $C_0 = C_{0,0}$, to the position along the streamline where $C_0 = C_{0,\mathrm{lim}}$. This specific position is identified by the travel time $\tau = \tau_{\mathrm{lim}}$. In the remaining part of the streamline, aerobic processes are assumed to switch off because the environment becomes anaerobic. Consequently, $\tau_{\mathrm{lim}}$ uniquely identifies the position along the streamline where the processes switch from aerobic to anaerobic. The evolution of $C_0$ along the streamline is provided by equation (B1), which solved with respect to $\tau_{\mathrm{lim}}$ after imposing $C_0(\tau_{\mathrm{lim}}, t) = C_{0,\mathrm{lim}}$ leads to the following expression for $\tau_{\mathrm{lim}}$:

$$\tau_{\mathrm{lim}} = \frac{1}{K_{RN(T)}} \cdot \ln\left(\frac{C_{0,0}}{C_{0,\mathrm{lim}}}\right). \quad (11)$$

This solution coincides with that obtained by *Marzadri et al.* [2011] under the hypothesis of negligible longitudinal dispersion.

[18] The prevailing aerobic or anaerobic conditions within the hyporheic zone influence the biogeochemical processes occurring along the streamlines and in turn the nitrogen removal efficiency of the streambed sediments. There are several ways to define the efficiency of the hyporheic zone in removing ammonium and/or nitrate. Here, we adopt the following two definitions:

$$R^{HZ}_i = \frac{Q^i_{M,dw}(t) - Q^i_{M,uw}(t)}{Q^i_{M,dw}(t)}, \quad i = 1, 2 \quad (12)$$

and

$$R^{S}_i = \frac{Q^i_{M,dw}(t) - Q^i_{M,uw}(t)}{C_{i,0} Q_S}, \quad i = 1, 2, \quad (13)$$

where $Q_S$ is the stream discharge. Equation (12) represents the efficiency of the hyporheic zone in removing the Nr species, evaluated with respect to the mass flux of the same species entering through the downwelling surface, while equation (13) represents the efficiency with respect to the mass flux in the stream.

[19] Furthermore, we define the normalized production of nitrogen gases as follows:

$$P^{HZ}_i = \frac{Q^i_{M,dw}(t) - Q^i_{M,uw}(t)}{Nr_0 Q_{dw}(t)}, \quad i = 3, 4, \quad (14)$$

which is normalized by the total downwelling Nr mass flux $(C_{1,0} + C_{2,0}) Q_{dw}(t) = Nr_0 \int_{A_{dw}} q(0)\, dA$.

### 2.4. Comparison With Field Measurements

[20] Before analyzing the impact of river morphology on the nitrogen cycle we verify our model against the experimental data published by *Beaulieu et al.* [2008, 2009]. To our best knowledge, these are the only works reporting both morphodynamic and nutrient concentration data needed for the application of our models without resorting to some type of fitting of the model on measured output data. This analysis complements the comparison performed by *Marzadri et al.* [2011] with the same data set but neglecting local dispersion and allows detecting the effect of local dispersion on Nr transformation within the hyporheic zone.

[21] Morpho-hydrodynamic (water discharge $Q$, stream velocity $v$ and water depth $Y_0$) and biogeochemical parameters

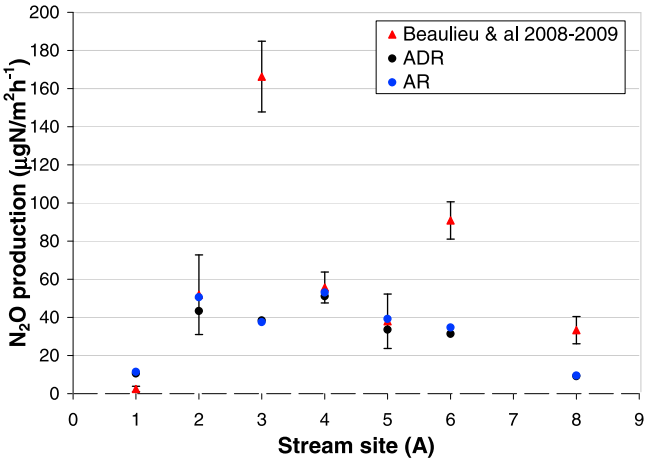


**Figure 3.** Comparison of the areal production of nitrous oxide obtained using the ADR model developed in this study with the AR model proposed by *Marzadri et al.* [2011] and field data published in studies by *Beaulieu et al.* [2008, 2009].

used in modeling the field measurements are published in the work of *Marzadri et al.* [2011].

[22] Figure 3 shows the comparison of nitrous oxide ($N_2O$) production computed with our models with measurements in 7 streams, whose characteristics are reported in the papers by *Beaulieu et al.* [2008, 2009] and *Marzadri et al.* [2011]. Both purely advective (AR) model developed by *Marzadri et al.* [2011], and advective-diffusive (ADR) model, developed here, well match the observed values with some large differences in streams 3 and 6 as previously observed by *Marzadri et al.* [2011]. Differences between the AR and ADR are small, thereby supporting the hypothesis that advection dominates solute transport within the hyporheic zone and local dispersion is of secondary importance, with respect to the impact of uncertainty of the measurements as reported by *Beaulieu et al.* [2008, 2009] and shown by the 95% error bars in Figure 3. However, local dispersion may be important under non-steady-state conditions, such as with varying solute loads and discharges of the stream flow. Whereas, the neglected transverse component of the local dispersion may be important in mixing hyporheic with groundwaters along the fringe between hyporheic zone and the underlying aquifer. Evaluating these effects is beyond the scope of this work.

## 3. Results

### 3.1. Simulation Setup

[23] Alternate-bar morphology can be described synthetically through three dimensionless parameters: the relative submergence $d_s = d_{50}/Y_0$, the Shields number $\theta$ (an index of sediment mobility), and the aspect ratio $\beta = B/Y_0$ [*Colombini et al.*, 1987]. In the present work, in order to analyze how different hydraulic and morphodynamic characteristics control the hyporheic inorganic nitrogen cycle, we explore a wide range of bedform topographies by letting $d_s$ to vary between 0.01 and 0.03, while keeping the other two parameters constant and equal to $\beta$ = 15 and $\theta$ = 0.08. All the computations are performed with $d_{50}$ = 0.01 m, such that variations of $d_s$ are obtained by varying the flow depth $Y_0$. Table 1, shows the depths $Y_0$ used in the simulations and the corresponding stream's characteristics computed by using classic morphological expressions [e.g., *Colombini et al.*, 1987]. Our analysis spans a wide range of channel's width ($2B$ = 1.5–30 m), slopes ($s_0$ = 0.13–2.64 %), and discharges ($Q_S$ = 0.07–51.9 $m^3/s$) (Table 1) and can be considered as representative of a large class of streams. In addition, Table 2 reports the biogeochemical parameters used in the simulations with the reaction rates derived from published field measurements [*Rutherford*, 1994; *Sjodin et al.*, 1997; *Dent and Henry*, 1999].

### 3.2. Morphodymanic Control on Hyporheic Residence Time

[24] The median hyporheic residence time $\tau_{up,50}$, for which 50% of the streamlines have a residence time shorter than its value, is a good index of the time available for biochemical reactions to occur within the hyporheic zone [*Tonina and Buffington*, 2011]. Figure 4 shows the dimensionless median residence time $\tau^*_{up,50} = \tau_{up,50}/t_f$, where $t_f$ is a suitable advective characteristics time scale, versus the dimensionless depth

**Table 1.** Morphological and Hydrodynamic Parameters Considered in the Simulations[a]

| Test | 1 | 2 | 3 | 4 | 5 | 6 | 7 | 8 | 9 | 10 |
|---|---|---|---|---|---|---|---|---|---|---|
| $H_{BM}$ (m) | 0.26 | 0.31 | 0.32 | 0.34 | 0.35 | 0.39 | 0.41 | 0.44 | 0.46 | 0.49 |
| $2B = z_d$ (m) | 1.5 | 2 | 2.14 | 2.31 | 2.5 | 3 | 3.33 | 3.75 | 4.29 | 5 |
| $Y_0$ (m) | 0.05 | 0.07 | 0.07 | 0.08 | 0.08 | 0.1 | 0.11 | 0.13 | 0.14 | 0.17 |
| $L$ (m) | 10.11 | 13.29 | 14.19 | 15.22 | 16.42 | 19.53 | 21.58 | 24.15 | 27.43 | 31.81 |
| $s_0$ (%) | 2.64 | 1.98 | 1.85 | 1.72 | 1.58 | 1.32 | 1.19 | 1.06 | 0.92 | 0.79 |
| $Q_S$ ($m^3$ $s^{-1}$) | 0.07 | 0.13 | 0.15 | 0.18 | 0.21 | 0.32 | 0.41 | 0.53 | 0.72 | 1.02 |
| Test | 11 | 12 | 13 | 14 | 15 | 16 | 17 | 18 | 19 | 20 |
| $H_{BM}$ (m) | 0.53 | 0.58 | 0.65 | 0.77 | 0.87 | 0.9 | 0.93 | 0.96 | 1 | 1.05 |
| $2B = z_d$ (m) | 6 | 7.5 | 10 | 15 | 20 | 21.43 | 23.08 | 25 | 27.27 | 30 |
| $Y_0$ (m) | 0.2 | 0.25 | 0.33 | 0.5 | 0.67 | 0.71 | 0.77 | 0.83 | 0.91 | 1 |
| $L$ (m) | 37.92 | 47.1 | 62.46 | 93.42 | 124.74 | 133.74 | 144.17 | 156.36 | 170.82 | 188.24 |
| $s_0$ (%) | 0.66 | 0.53 | 0.4 | 0.26 | 0.2 | 0.19 | 0.17 | 0.16 | 0.15 | 0.13 |
| $Q_S$ ($m^3$ $s^{-1}$) | 1.53 | 2.51 | 4.73 | 11.51 | 21.56 | 25.06 | 29.46 | 39.96 | 42.24 | 51.97 |

[a]Relationships with reference parameters are also indicated: mean flow depth $Y_0 (= d_{50}/d_s)$; channel width $2B (= 2Y_0\,\beta)$; alluvium depth $z_d$; streambed slope $s_0 (= \theta\,\Delta\,d_s)$, where $\Delta$ = 1.65 is the submerged specific gravity of the sediment; stream water discharge $Q_S = C_C\,\beta\,s_0^{(1/2)}\,Y_0^{(5/2)}$, where $C_C = C_z g^{1/2}$ is the roughness coefficient, with $C_z$ indicating the dimensionless Chezy coefficient $C_z = 6 + 2.5\ln\left(\frac{1}{2.5d_s}\right)$ and $g$ the gravitational acceleration; bed form length $L$; and bar amplitude $H_{BM}$. Note that in all cases we fixed $z_d = 2B$, $d_{50}$ = 0.01 m and $\beta$ = 15.

**Table 2.** Physical and Biogeochemical Parameters Used in the Simulations

| Parameter | Unit | Test A | Test B | Test C |
|---|---|---|---|---|
| Relative Concentration | [−] | 0.3 | 1.10 | 4.1 |
| $D_L$ | ($m^2/s$) | $10^{-6}$ | $10^{-6}$ | $10^{-6}$ |
| $C_{0,0}$[a] | (mg/l) | 10 | 10 | 10 |
| $C_{0,\lim}$[a] | (mg/l) | 4 | 4 | 4 |
| $C_{1,0}$ | (mg/l) | 0.374[b] | 1.458 | 5.460 |
| $C_{2,0}$ | (mg/l) | 1.325[b] | 1.325 | 1.325 |
| $Nr_0$ | (mg/l) | 1.699 | 2.783 | 6.785 |
| $C_{3,0}$ | (mg/l) | 0.0 | 0.0 | 0.0 |
| $C_{4,0}$ | (mg/l) | 0.0 | 0.0 | 0.0 |
| $K_R^{(20)a}$ | ($d^{-1}$) | 0.10 | 0.10 | 0.10 |
| $K_N^{(20)b}$ | ($d^{-1}$) | 3.46 | 3.46 | 3.46 |
| $K_C^{(20)c}$ | ($d^{-1}$) | 1.0 | 1.0 | 1.0 |
| $K_D^{(20)b}$ | ($d^{-1}$) | 1.65 | 1.65 | 1.65 |
| $\varphi_R^{(20)a}$ | (−) | 1.047 | 1.047 | 1.047 |
| $\varphi_N^{(20)b}$ | (−) | 1.040 | 1.040 | 1.040 |
| $\varphi_C^{(20)c}$ | (−) | 1.047 | 1.047 | 1.047 |
| $\varphi_D^{(20)b}$ | (−) | 1.045 | 1.045 | 1.045 |

[a]Reported in *Rutherford* [1994].
[b]Reported in *Sjodin et al.* [1997].
[c]Reported in *Dent and Henry* [1999].

$Y^*_{BM} = Y_0/H_{BM}$ for different values of hydraulic conductivity, $K$. We use here the expression of $Y^*_{BM}$ derived from *Colombini et al.* [1987] for alternate bar morphology

$$Y^*_{BM} = \left[ b_1 \left( \frac{\beta - \beta_C}{\beta_C} \right)^{\frac{1}{2}} + b_2 \left( \frac{\beta - \beta_C}{\beta_C} \right) \right]^{-1}, \qquad (15)$$

where $\beta_c$ is the threshold value of the aspect ratio $\beta$ for alternate-bar formation and $b_1$ and $b_2$ are functions of the flow field and sediment characteristics [see *Colombini et al.*, 1987, Figures 5–6]. Furthermore, the time scale is $t_f = L/(K\, s_0 C_z)$, where $s_0$ is the bed slope, $C_z$ is the dimensionless Chezy coefficient and $L$ is the bed form wavelength [*Marzadri et al.*, 2010]. Notice that we assumed $L$ and $K\, s_0$ as length and velocity scales of the hyporheic exchange, respectively. The Chezy coefficient accounts for streambed roughness, which affects surface water elevation and consequently near-bed pressure distribution. The later is the primary driver of the hyporheic flow for this type of bed form [*Tonina and Buffington*, 2007, 2009a; *Marzadri et al.*, 2010].

[25] As expected, $\tau^*_{up,50}$ is insensitive to $K$ as a consequence of the linearity of Darcy's equation, such that a variation of $K$ causes a proportional variation of the travel times, and of $t_f$ as well (Figure 4). However, nonlinear effects are expected in case $K$ is spatially variable (heterogeneous). Whereas $\tau^*_{up,50}$ increases with $Y^*_{BM}$, the coefficient of variation $CV = \sigma_{\tau_{up}}/\mu_{\tau_{up}}$, where $\mu_{\tau_{up}}$ is mean and $\sigma_{\tau_{up}}$ the standard deviation of the travel time, remains approximately constant around a value of 1.3. A similar value (i.e., $CV = 1.4$) was observed by *Tonina and Buffington* [2011] in flume experiments with fully submerged bars of small amplitude. This rather high $CV$ indicates a wide distribution of residence times experienced by the solutes emerging from the upwelling area, which is therefore expected to exert a strong influence on biogeochemical transformations. In addition, the strong relationship we found here between the residence time distribution and the morphological characteristics of streambed have been also observed experimentally in branches of the Mississippi-Missouri river network [*Mulholland et al.*, 2008]. This connection cannot be established with a purely diffusional zero-dimensional exchange model, often used in modeling the hyporheic exchange.

[26] The dimensionless median residence time, $\tau^*_{up,50}$, can be used to identify streams, whose morphodynamic characteristics result in comparable residence time distributions and therefore showing comparable effects on Nr species. We observe that $\tau^*_{up,50}$ is proportional to $Y^*_{BM}$ such that it increases from small and steep to large low-gradient streams. Therefore, our model captures what already observed in river systems, i.e., that Nr cycling changes from low to high order streams along river networks [*Alexander et al.*, 2000; *Peterson et al.*, 2001].

[27] The following exponential function well approximates $\tau^*_{up,50}$ obtained with our model for fully submerged alternate bar topography (Figure 4):

$$\tau^*_{up,50} = 0.21 e^{1.22 Y^*_{BM}}, \qquad (16)$$

with $R^2 = 0.99$, which quantifies the effect of streambed morphology, epitomized by the dimensionless depth ($Y^*_{BM}$), on the residence time within the alluvial sediments.

[28] Equation (16) expresses $\tau^*_{up,50}$ as a function of physical quantities (e.g., mean water depth, streambed slope, stream width, bed form amplitude and wavelength, sediment hydraulic conductivity and median sediment grain size) which are available, or can be obtained with a limited effort, and allows correlating hyporheic travel time characteristics to river and sediment hydraulic properties. Although, we derive this relationship under the hypothesis of equilibrium conditions between flow regime and streambed morphology, the work of *Marzadri et al.* [2010] shows that it is applicable for any discharge that entirely submerges the gravel bars.

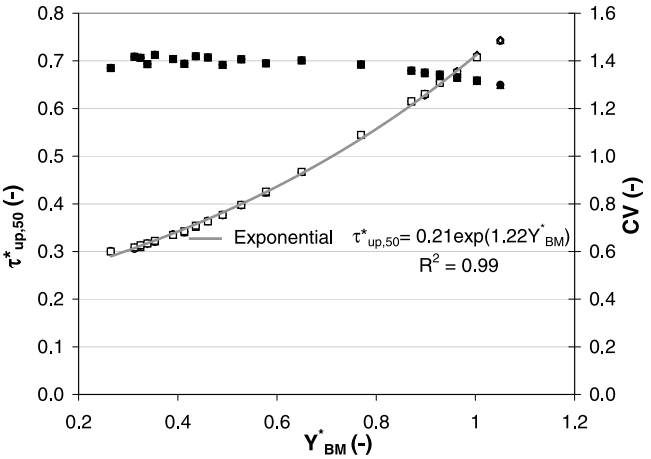


**Figure 4.** Dimensionless median residence time $\tau^*_{up,50} = \tau_{up,50} K s_0 C_z / L$ (open symbols) and coefficient of variation $CV = \sigma_{\tau_{up}}/\mu_{\tau_{up}}$ (solid symbols) as a function of the dimensionless depth $Y^*_{BM}$ for different values of hydraulic conductivity $K$. Simulations have been conduced with the following values of hydraulic conductivity: $K = 0.01$ m/s (diamonds), $K = 0.005$ m/s (triangles), $K = 0.001$ m/s (circles) and $K = 0.0001$ m/s (squares). Because of the normalization, results for $\tau^*_{up,50}$ and $CV$ with different $K$ collapse along a single line; thus all the symbols overlap and only the squares are visible.

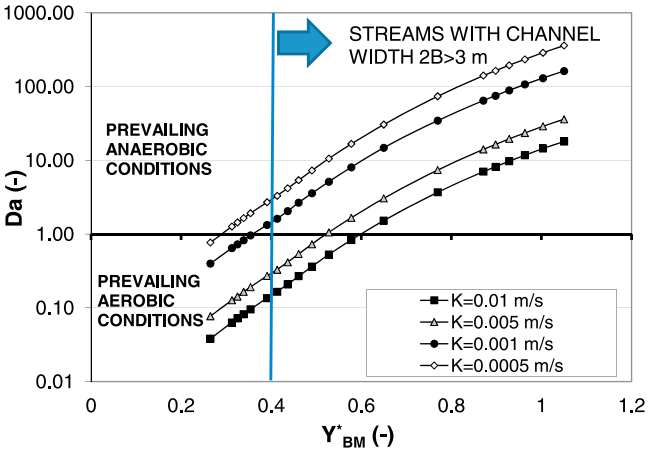


**Figure 5.** Damköhler number $Da = \tau_{up,50}/\tau_{\lim}$ as a function of the dimensionless depth $Y^*_{BM} = Y_0/H_{BM}$ for different values of hydraulic conductivity $K$.

### 3.3. Hyporheic Aerobic-Anaerobic Zones

[29] Geochemical transformations occurring in the hyporheic zone depend on the reciprocal values assumed by the residence time of solutes and the time needed to reach the anoxic conditions as expressed by the ratio $\tilde{\tau} = \tau/\tau_{\lim}$, between the residence time, which in stationary conditions coincides with the travel time of the particle traveling along the streamline, and the time needed to deplete oxygen concentration $C_{0,\lim}$. $\tilde{\tau}$ indicates whether at a given position along the streamline redox conditions are aerobic ($\tilde{\tau} < 1$) or anaerobic ($\tilde{\tau} > 1$).

[30] With these considerations in mind, we introduce a dimensionless number defined as the ratio between the median residence time ($\tau_{50}$) evaluated at a control surface within the hyporheic zone and the residence time limit ($\tau_{\lim}$) at which oxygen concentration is depleted to $C_{0,\lim}$: $\tilde{\tau}_{HZ} = \tau_{50}/\tau_{\lim}$. This new metric provides an immediate indication of the prevailing conditions within the hyporheic zone from the downwelling area to the compliance surface, which can be the upwelling area, or any other control surface internal to the hyporheic zone. Values of $\tilde{\tau}_{HZ} < 1$ are indicative of prevailing aerobic conditions upstream, while $\tilde{\tau}_{HZ} > 1$ indicates that more than 50% of the streamlines are already in anaerobic conditions at the point where they cross the compliance surface. An indication of the global geochemical status of the hyporheic zone is therefore provided by the following dimensionless Damköhler number: $Da = \tau_{up,50}/\tau_{\lim}$. Consequently, values of $Da$ larger than 1 indicate prevailing anaerobic conditions, whereas values smaller than 1 prevailing aerobic conditions, within the hyporheic sediment between the downwelling and upwelling surfaces. This allows analyzing the prevailing redox conditions within the hyporheic zone induced by alternate-bar morphology as a function of stream size as shown in Figure 5, which depicts $Da$ as a function of $Y^*_{BM}$. In our simulations, transition between prevailing aerobic and prevailing anaerobic conditions occurs for $Y^*_{BM}$ between 0.3 and 0.6 depending on hydraulic conductivity of the streambed material. For given hydraulic and biogeochemical characteristics of the sediment (i. e. for a given curve in Figure 5), $Da$ increases passing from small to large streams implying that the fraction of the hyporheic zone in anaerobic conditions increases with stream size. Notice that the surface separating aerobic from anaerobic portions of the hyporheic zone can be identified by detecting the points along the streamlines where $\tilde{\tau} = 1$; the volume upstream of this surface is in aerobic condition, while that downstream is in anaerobic condition.

[31] The above results are in line with the experimental findings of *Triska et al.* [1993] along a reach of the Little Lost Man Creek, California, where they observed low concentrations of dissolved oxygen and nitrate in zones with long travel times, where likely $\tilde{\tau} > 1$, while both species were present at higher concentrations in zones with short travel times ($\tilde{\tau} < 1$) i.e., close to the downwelling area. Furthermore, the study of *Krause et al.* [2009] highlights the importance of the residence time on denitrification efficiency, which increases with long residence times within the hyporheic zone as the anaerobic portion of the hyporheic zone becomes dominant with respect to the aerobic portion. Most recently, *Zarnetske et al.* [2011] measured that dissolved oxygen below one parafluvial gravel bar decreases almost exponentially with hyporheic residence time. Our results are in qualitative agreement with this experimental findings because the length of the streamlines crossing the points along a vertical section increases with depth.

[32] Because $Da$ includes the effects of streambed morphology via $\tau_{up,50}$ and hyporheic biogeochemical properties via $\tau_{\lim}$, we use this index to study the effects of alternate-bar morphology in our analysis.

### 3.4. Ammonium and Nitrate Removal

[33] Figure 6a shows the efficiency, $R_1^S$, in transforming $NH_4^+$ to $NO_3^-$, evaluated with respect to the stream mass flux, as a function of $Da$ for both the ADR, (see equation (A3) in Appendix A), and the simplified AR models. Figure 6b repeats Figure 6a for the efficiency $R_1^{HZ}$, evaluated with respect to the downwelling mass flux. The physical, chemical, and geomorphological parameters used in the simulations are reported in Table 2. Differences between the two models are small regardless of residence time. This shows that mixing due to local dispersivity influences only marginally the global transformation of $NH_4^+$ to $NO_3^-$ occurring within the hyporheic zone, although locally larger differences may be observed. The hyporheic zone is always a sink of ammonium irrespective to $RC$ ($RC < 1$ for streams richer in nitrate than ammonium). This is in line with field measurements conducted by *Fernald et al.* [2006] in a gravel bed river. Both models show $R_1^S$ decreasing with $Da$, thus with stream dimension and inversely with bacterial activities (represented by $\tau_{\lim}$), again irrespective to $RC$. Efficiency is greater for $RC > 1$ because of the predominance of ammonium with respect to nitrate in the stream water. For a fixed value of $\tau_{\lim}$ and $K$, $Da$ increase with the stream dimension and consequently with the stream water discharge. Therefore, the reduction of $R_1^S$ with $Da$ is mainly due to the increase of stream discharge, which we use to normalize ammonium transformation in the definition of $R_1^S$.

[34] Conversely, $R_1^{HZ}$ increases with $Da$ because of the longer time available for nitrification and reaches a constant value for $Da \approx 10$. The transport model has a marginal

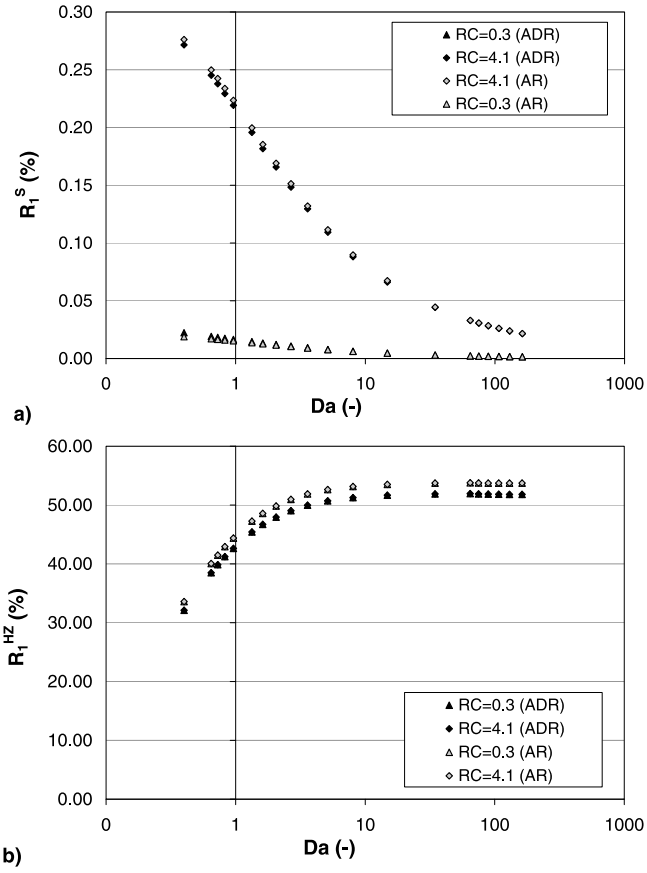


**Figure 6.** Transformation of ammonium within the hyporheic zone relative to (a) stream ammonium mass flux, $R_1^S$, and (b) downwelling ammonium mass flux, $R_1^{HZ}$, versus the Damköhler $Da = \tau_{up,50}/\tau_{\lim}$ for streams initially richer with nitrate RC < 1 and ammonium RC > 1. Both ADR and AR solutions are shown.

effect on transformation of ammonium, with ADR predicting a slightly smaller value of $R_1^S$ than AR, because diffusion lowers local solute concentrations, thereby reducing the overall reaction rates. Lower concentrations result in lower transformations and therefore a higher export of solute from the hyporheic zone through the upwelling surface. The difference between $R_1^S$ obtained with ADR and AR models decreases with *RC* due to lower initial ammonium concentrations in the stream.

[35] Figures 7a and 7b show the two efficiency indexes $R_2^S$ and $R_2^{HZ}$ for nitrate removal predicted with the ADR (A4) model as a function of *Da*. AR produces similar results, which are not reported here. Figure 7a shows $R_2^S$ for three different streambed hydraulic conductivity values and for $RC = 0.3$ and $RC = 3$. Large hydraulic conductivities increase downwelling mass fluxes and thus the amount of nitrate subject to denitrification. The efficiency $R_2^S$, evaluated with respect to the stream mass flux, increases with *K*, which has a double effect because it acts also on the mean dimensionless time and consequently on *Da* distribution (as previously commented in Figure 5). We observe that $R_2^S$ increases reaches a maximum and then decreases with *Da*, suggesting that there is a particular streambed geometry, which maximizes nitrate removal. The reduction of $R_2^S$ at large *Da* after the peak is due to the combined effect of the upper limit of the removal evidenced in Figure 7b and the increase of mass flux in the stream associated to the increase of water discharge. In fact, in our simulations *Da* increases with the water discharge when $\tau_{\lim}$ and *K* are kept constant.

[36] When the stream water is richer in $NO_3^-$ than in $NH_4^+$ (i.e., $RC = 0.3$), $R_2^S$ is always positive and thus the hyporheic zone is a sink of nitrate. On the other hand, when the stream water is richer in $NH_4^+$ than $NO_3^-$ (i.e., for $RC = 3$) and for relatively small *Da* values, nitrate produced by nitrification of ammonium is larger than that removed in the anaerobic portion of the hyporheic zone. This causes $R_2^S$ to assume negative values, which indicates production of nitrate. However, as *Da* increases, denitrification removes more and more nitrate and $R_2^S$ increases, reaches a maximum and then decreases due to the parallel increase of water discharge. Similarly, $R_2^{HZ}$ shows that hyporheic zone is always a sink of nitrate for small values of relative concentration ($RC = 0.3$). Because of this behavior we can identify a

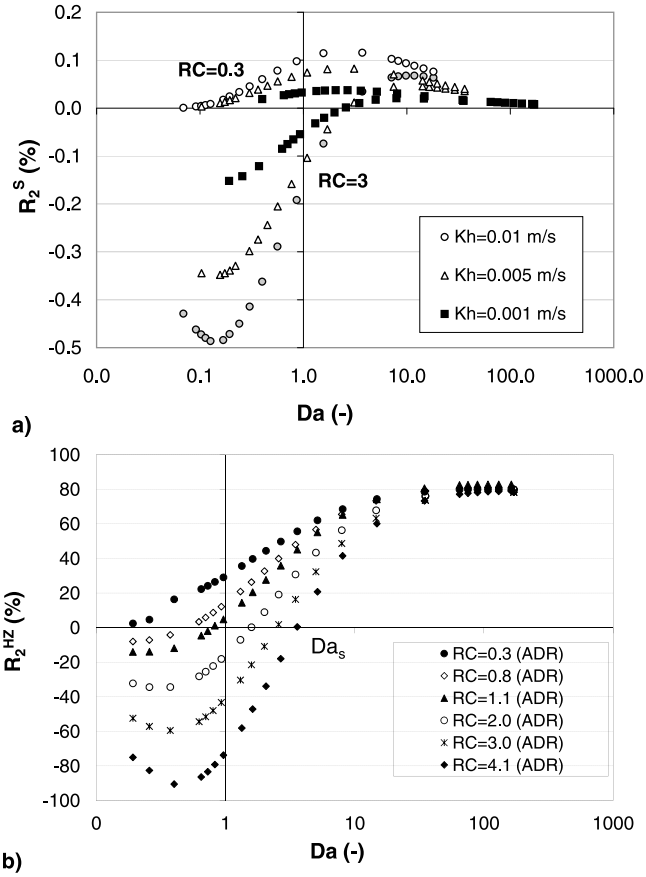


**Figure 7.** Removal of nitrate within the hyporheic zone relative to (a) stream nitrate mass flux, $R_2^S$, and (b) downwelling nitrate mass flux, $R_2^{HZ}$, computed with the ADR model versus the Damköhler $Da = \tau_{up,50}/\tau_{\lim}$ in stream initially rich with nitrate $RC < 1$ (open symbols) and ammonium $RC > 1$ (solids symbols), for different values of hydraulic conductivity (top) and for a constant value of hydraulic conductivity $K = 0.001$ m/s (bottom).

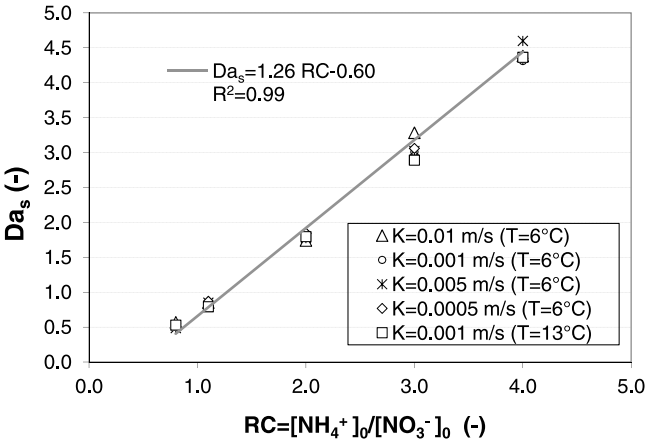


**Figure 8.** $Da_s$ as a function of the stream relative concentration ($RC$) for several values of the hydraulic conductivity $K$ and two temperatures ($T$ = 6°C and $T$ = 13°C). The linear regression equation is valid for $RC > 0.48$ and for the reaction rate of biomass uptake and denitrification reported in Table 2.

particular value of $Da$, which we call $Da_s$, above which the hyporheic zone acts as a sink of $NO_3^-$. $Da_s$ is only a function of $RC$ and not of streambed hydraulic conductivity (at least for a spatially uniform hydraulic conductivity) and temperature (Figure 8). Therefore, all reaches of streams with $Da > Da_s$ are sinks of $NO_3^-$.

[37] Experimental studies conducted in a gravel bed river by *Fernald et al.* [2006] also confirm that the hyporheic zone may act as a source or a sink for $NO_3^-$ depending on the hyporheic flow rate $q_H$, which is an index of hyporheic residence time, such that streams with low $q_H$ are in prevailing anaerobic conditions and consequently the hyporheic zone acts as sink for nitrate. Field measurements conducted by *Zarnetske et al.* [2011] show similar results with nitrification producing $NO_3^-$ at short residence times and denitrification removing $NO_3^-$ at long residence time. As in our model the transition occurs when dissolved oxygen reaches a threshold value, which is assumed 0.2 mg/l in their field observations.

[38] Similarly to $R_1^{HZ}$, the efficiency, $R_2^{HZ}$ evaluated with respect to the downwelling mass flux of nitrate, reaches a maximum value smaller than 100%. This maximum value depends on the residence time distribution; the relatively high values of $CV$ suggests that there will be always streamlines in aerobic conditions such that not all the mass flux of nitrate entering the hyporheic zone can be removed and the efficiency should be smaller than 100%.

### 3.5. Temperature Effects

[39] Water temperature plays an important role in biogeochemical processes because reaction kinetics are temperature dependent. The effect of temperature on the dimensionless production of nitrous oxide, $P_4^S$, in the stream water, is shown in Figure 9 as a function of $Da$ for both AR and ADR models and with $T$ = 6°C and $T$ = 13°C. The flux concentration of nitrous oxide $C_4$ is evaluated with equations (B6), (6) and (9). In all cases $RC$ = 0.3, such that the initial pulse is richer in $NO_3^-$ than $NH_4^+$.

[40] High temperatures increase the reaction rate coefficient according to Arrhenius law (equation (5)) and consequently the production of molecular nitrogen. However, the figure shows that $P_4^{HZ}$ is less sensitive to the water temperature when $Da$ is large, i.e., for large residence times or fast reaction rate (small $\tau_{\lim}$). For given stream Nr concentrations and constant $\tau_{\lim}$, large streams (large $Da$) produce larger quantities of nitrogen gases than small streams, irrespective of water temperature, because of the prevailing anaerobic conditions along the streamlines. However, the emission relative to the nutrients load in the stream, $P_4^S$, reduces as an effect of the increase of stream discharge. Conversely, because of the shorter residence times temperature variations have a stronger impact in small steep than in large low-gradient streams as shown in Figure 9 for intermediate $Da$ results.

[41] This implies that small steep and large low-gradient streams respond differently to seasonal temperature changes in temperate regions. Small steep streams produce more $N_{gas}$ during the warm season, while smaller differences with respect to the cold season are expected for large low-gradient streams. This may suggest that field measurements and monitoring procedure of nutrients should account for seasonal variations but also for the daily cycle as temperatures may vary remarkably between day and night in small streams where typically these measurements are taken. Additionally, biomass nitrate uptake could potentially increase with temperature much faster than denitrification rates in some systems. Consequently, biomass uptake could lower the available nitrate for denitrification and hence it could offset the observed increase in $P_4^S$ with temperature.

## 4. Conclusions

[42] Our analysis based on analytical solutions of a multispecies reactive solute transport within the hyporheic zone presents several results:

[43] 1. The ratio between a representative hyporheic residence time, whose value depends on the scale of the analysis, and the characteristic time of oxygen consumption, $\tau_{\lim}$,

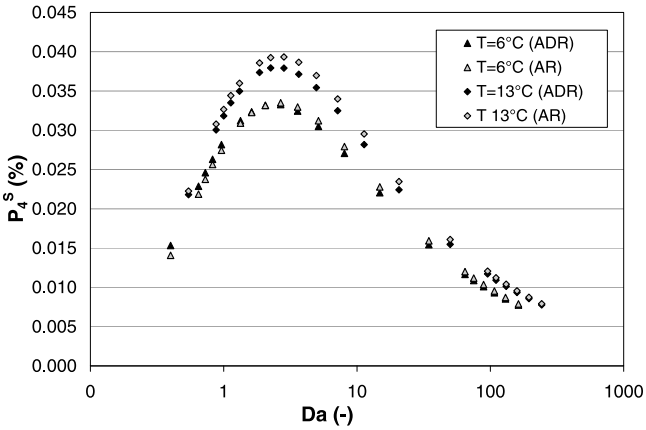


**Figure 9.** Effects of hyporheic water temperature on the dimensionless production of nitrous oxide, $P_4^S$, within the stream versus the Damköhler $Da = \tau_{up,50}/\tau_{\lim}$. In all cases $RC$ = 0.3 and $K$ = 0.001 m/s.

can be used to identify the aerobic and anaerobic zonation of the hyporheic zone.

[44] 2. A new Damköhler number, *Da*, defined as the ratio between the median hyporheic residence time, $\tau_{up,50}$ and $\tau_{\lim}$ can be used to identify the prevailing aerobic ($Da < 1$) or anaerobic ($Da > 1$) conditions at the scale of a single bedform.

[45] 3. Streambed morphology and flow by influencing *Da* have a strong control on redox conditions within the hyporheic zone.

[46] 4. Hyporheic efficiency in removing ammonium and nitrate increases with *Da* such as nitrous oxide production.

[47] 5. A particular value of *Da*, $Da_s$, which does not depend on streambed hydraulic conductivity, for homogenous hydraulic properties of the sediment, and on hyporheic temperature but only on the relative abundance of ammonium and nitrate, defines when the hyporheic zone is a source or a sink of nitrate.

[48] 6. Hyporheic efficiency in removing ammonium and nitrate is lower than 100% in streams with alternate-bar morphology due to the large distribution of residence time induced by this topography.

[49] 7. Diffusion is of secondary importance compared to advection in the transformation and removal of reactive nitrogen within the hyporheic zone.

[50] 8. Hyporheic water temperature affects nitrogen transformation in systems with small but not for those with large *Da* values.

[51] Our proposed Lagrangian approach applied at the single streamline suggests that the dimensionless number $\widetilde{\tau} = \tau/\tau_{\lim}$, where $\tau$ is the residence time of the flow path, can be used to determine whether the flow path has prevailing aerobic ($\widetilde{\tau} < 1$) or anaerobic ($\widetilde{\tau} > 1$) conditions. If the analysis is restricted over a portion of the hyporheic zone, a dimensionless travel time could be defined as $\widetilde{\tau}_{HZ} = \tau_{50}/\tau_{\lim}$, where $\tau_{50}$ is the median residence time evaluated at a control surface within the hyporheic zone. For instance, the analysis could be applied to a portion of the hyporheic zone as defined in the work of *Gooseff* [2010].

[52] At the bedform scale, our results show a strong dependance between nitrification-denitrification processes and alternate-bar morphology. Through equations (16) and (11) we define a new Damkhöler number $Da = \tau_{up,50}/\tau_{\lim}$ able to represent this interaction between biogeochemical and morphological processes.

[53] Consequently, this Lagrangian approach can be extended to any other bed forms provided that $\tau_{up,50}$ can be obtained. For instance, this analysis could be readily applied to dune-like bedform for which solutions of the residence time distribution are available [e.g., *Elliott and Brooks*, 1997; *Bottacin-Busolin and Marion*, 2010] or for studying localized hyporheic flow such as that induced by logs [*Sawyer et al.*, 2011].

[54] *Da* values lower than 1 results in prevailing aerobic conditions with low reactive nitrogen removal at the unit scale. Values of *Da* larger than 1 indicate prevailing anaerobic condition with large opportunity of Nr removal and production of nitrogen gases. As a result, the hyporheic zone may be an important source of $N_2O$ to stream waters and may play a significant role regulating greenhouse gas emissions and consequently the greenhouse effect.

[55] Application of *Da* for increasing stream size with alternate-bar morphology, shows different roles between hyporheic zones of mountain headwaters, which are typically small and steep streams, and those of large low-gradient streams, typical of valley bottoms. Nitrification processes dominate in the former streams because of short residence times whereas denitrification plays a major role in the latter streams. Emissions of nitrogen gases increase with temperature in small steep streams such that they are more efficient in removing nitrate during the warm than cold season. Conversely, streams at the valley bottom can act as sinks of nitrate and source of nitrogen gases with similar efficiency regardless of seasonal or daily temperature variations.

## Appendix A: Biogeochemical Model

### A1. Dissolved Oxygen

[56] Dissolved oxygen transport and transformation within the hyporheic zone is modeled by specializing equation (10) for $i = 0$:

$$\begin{cases} \dfrac{\partial C_0}{\partial \tau} + \dfrac{\partial C_0}{\partial t} = \dfrac{D_L}{u^2}\dfrac{\partial^2 C_0}{\partial \tau^2} + f_0 \\ C_0(\tau, 0) = C_{0,\lim}, \\ C_0(0, t) = C_{0,0}, \\ \dfrac{\partial C_0}{\partial \tau}\Big|_{\tau\to\infty} = 0 \end{cases} \tag{A1}$$

with

$$f_0 = -K_{RN(T)} C_0, \tag{A2}$$

where $K_{RN(T)}$ is the oxygen rate coefficient that accounts for respiration and nitrification. For simplicity and without loosing generality, we assume that $C_0$ is at saturation in the stream waters at all time such that $C_{0,0} = 10$ mg/l in all simulations. Furthermore, $C_0 = C_{0,\lim}$ at $t = 0$ within the hyporheic zone, and $\dfrac{\partial C_0}{\partial \tau} = 0$ for long residence times (i.e., for $\tau \to \infty$).

### A2. Nr Species

[57] The streamline is divided into two parts: in the first part, which is identified with $\tau \le \tau_{\lim}$, a solution is obtained by assuming $K_D = 0$ (denitrification is switched off) and imposing only the boundary condition at the downwelling surface. In the second part (i.e., for $\tau > \tau_{\lim}$), the solution is obtained by assuming $K_N = K_C = 0$ and imposing the boundary condition at the upwelling surface. The two remaining constants are obtained by simply imposing that the two expressions of the concentration assume the same values at the interface between these two zones (i.e., for $\tau = \tau_{\lim}$). Comparisons between accurate numerical simulations based on conservation of concentration fluxes, obtained by imposing $\dfrac{\partial C_{i,ox}}{\partial \tau}\Big|_{\tau\to\tau_{\lim}} = \dfrac{\partial C_{i,aox}}{\partial \tau}\Big|_{\tau\to\tau_{\lim}}$, where $C_{i,ox}$ and $C_{i,aox}$ are the two solutions obtained for $\tau < \tau_{\lim}$ and $\tau > \tau_{\lim}$, respectively, and our simplified analytical solution, obtained by imposing $\dfrac{\partial C_{i,ox}}{\partial \tau}\Big|_{\tau\to\infty} = 0$, show negligible differences. The error increases slowly with $\tau_{\lim}$ and we observe less than a 3% difference for $\tau_{\lim} = 8$ days.

[58] The dynamics of ammonium species can be obtained by solving the differential equation that results from specializing the governing equation (10) for $i = 1$ as follows:

$$\begin{cases} \dfrac{\partial C_1}{\partial \tau} + \dfrac{\partial C_1}{\partial t} = \dfrac{D_L}{u^2}\dfrac{\partial^2 C_1}{\partial \tau^2} + f_1, \\ C_1(\tau, 0) = 0, \\ C_1(0, t) = C_{1,0}, \\ \dfrac{\partial C_1}{\partial \tau}|_{\tau\to\infty} = 0. \end{cases} \tag{A3}$$

[59] Similar to the previous case, the evolution of $C_2$ can be obtained by solving the differential equation obtained by specializing the equation (10) for $i = 2$:

$$\begin{cases} \dfrac{\partial C_2}{\partial \tau} + \dfrac{\partial C_2}{\partial t} = \dfrac{D_L}{u^2}\dfrac{\partial^2 C_2}{\partial \tau^2} + f_2, \\ C_2(\tau, 0) = 0, \\ C_2(0, t) = C_{2,0}, \\ \dfrac{\partial C_2}{\partial \tau}|_{\tau\to\infty} = 0. \end{cases} \tag{A4}$$

In equations (A3) and (A4) the reaction terms $f_1$ and $f_2$ represent the interplay between oxygen, ammonium and nitrate and are modeled with the following Monod kinetics [*Bailey and Ollis*, 1977]:

$$\begin{cases} f_1 = -\mu_{N(T)}\dfrac{C_1}{K1_{N(T)} + C_1} \\ f_2 = -\mu_{C(T)}\dfrac{C_2}{K1_{C(T)} + C_2} - \mu_{D(T)}\dfrac{C_2}{K1_{D(T)} + C_2} - f_1 \end{cases}, \tag{A5}$$

where $\mu_{N(T)}$, $\mu_{C(T)}$ and $\mu_{D(T)}$ are the nitrification, biomass assimilation, and denitrification potential (maximum) rate, respectively and $K1_{N(T)}$, $K1_{C(T)}$, and $K1_{D(T)}$ their associated half-saturation (Monod) constants. Considering streams with low pollution [*Buss et al.*, 2006; *Kjellin et al.*, 2007] and consequently with low concentrations ($K1_i \gg [C_i]$) [*McLaren*, 1976; *Sheibley et al.*, 2003], equations (A5) simplify to the following first-order (linear) kinetics [*Marzadri et al.*, 2011]:

$$\begin{cases} f_1 = -K_{N(T)}C_1 \\ f_2 = -\left(K_{C(T)} + K_{D(T)}\right)C_2 - f_1 \end{cases} \tag{A6}$$

with

$$\begin{cases} K_{N(T)} = \dfrac{\mu_{N(T)}}{K1_{N(T)}} \\ K_{C(T)} = \dfrac{\mu_{C(T)}}{K1_{C(T)}}, \\ K_{C(T)} = \dfrac{\mu_{D(T)}}{K1_{D(T)}} \end{cases} \tag{A7}$$

where $K_{N(T)}$, $K_{C(T)}$, and $K_{D(T)}$ are the nitrification, biomass assimilation and denitrification rate coefficients, respectively.

[60] Finally, nitrogen gases are the products of denitrification processes and their concentration can be computed by solving the following equation:

$$\begin{cases} \dfrac{\partial C_3}{\partial \tau} + \dfrac{\partial C_3}{\partial t} = \dfrac{D_L}{u^2}\dfrac{\partial^2 C_3}{\partial \tau^2} + K_{D(T)}C_2, \\ C_3(\tau, 0) = 0, \\ C_3(0, t) = C_{3,0}, \\ \dfrac{\partial C_3}{\partial \tau}|_{\tau\to\infty} = 0. \end{cases} \tag{A8}$$

## Appendix B: Solution of the Advection-Dispersion Transport in the Hyporheic Zone

### B1. Dissolved Oxygen

[61] The solution of model (A1) assumes the following form:

$$\begin{aligned} C_0(\tau, t) = C_{0,\lim}\exp\left(-K_{RN(T)}t\right)\Bigg[1 - \frac{1}{2}erfc\left(\frac{u\tau - ut}{2\sqrt{D_L t}}\right) \\ - \frac{1}{2}\exp\left(\frac{u^2\tau}{D_L}\right)erfc\left(\frac{u\tau + ut}{2\sqrt{D_L t}}\right)\Bigg] \\ + \frac{1}{2}C_{0,0}\Bigg\{\exp\left[\frac{u^2\tau}{2D_L}\left(1 + \sqrt{1 + \frac{4K_{RN(T)}D_L}{u^2}}\right)\right] \\ \cdot efrc\left[\frac{u\tau + ut\sqrt{1 + \frac{4K_{RN(T)}D_L}{u^2}}}{2\sqrt{D_L t}}\right] \\ + \exp\left[\frac{u^2\tau}{2D_L}\left(1 - \sqrt{1 + \frac{4K_{RN(T)}D_L}{u^2}}\right)\right] \\ \cdot erfc\left[\frac{u\tau - ut\sqrt{1 + \frac{4K_{RN(T)}D_L}{u^2}}}{2\sqrt{D_L t}}\right]\Bigg\}. \end{aligned} \tag{B1}$$

### B2. Nr Species

[62] Along the aerobic part of the streamlines the solutions of the models (A3), (A4) and (A8) assume the following expressions:

$$\begin{cases} C_1(\tau, t)_{ox} = \dfrac{1}{2}C_{1,0} \quad C_{1,ox} \\ C_2(\tau, t)_{ox} = \dfrac{K_{N(T)}}{2\left(K_{C(T)} - K_{N(T)}\right)}C_{1,ox}(\tau, t) \\ \qquad + \dfrac{1}{2}\left(C_{2,0} - \dfrac{K_{N(T)}}{\left(K_{C(T)} - K_{N(T)}\right)}C_{1,0}\right)C_{2,ox} \\ C_4(\tau, t) = C_{4,0} \\ C_3(\tau, t) = 0 \end{cases}, \tag{B2}$$

where

$$\begin{cases} C_{1,ox} = \exp\left[\dfrac{u^2\tau}{2D_L}\left(1 + \sqrt{1 + \dfrac{4K_{N(T)}D_L}{u^2}}\right)\right]erfc\left(\dfrac{u\tau + ut\sqrt{1 + \frac{4K_{N(T)}D_L}{u^2}}}{2\sqrt{D_L t}}\right) \\ \qquad + \exp\left[\dfrac{u^2\tau}{2D_L}\left(1 - \sqrt{1 + \dfrac{4K_{N(T)}D_L}{u^2}}\right)\right]erfc\left(\dfrac{u\tau - ut\sqrt{1 + \frac{4K_{N(T)}D_L}{u^2}}}{2\sqrt{D_L t}}\right) \\ C_{2,ox} = \exp\left[\dfrac{u^2\tau}{2D_L}\left(1 + \sqrt{1 + \dfrac{4K_{C(T)}D_L}{u^2}}\right)\right]erfc\left(\dfrac{u\tau + ut\sqrt{1 + \frac{4K_{C(T)}D_L}{u^2}}}{2\sqrt{D_L t}}\right) \\ \qquad + \exp\left[\dfrac{u^2\tau}{2D_L}\left(1 - \sqrt{1 + \dfrac{4K_{C(T)}D_L}{u^2}}\right)\right]erfc\left(\dfrac{u\tau - ut\sqrt{1 + \frac{4K_{C(T)}D_L}{u^2}}}{2\sqrt{D_L t}}\right). \end{cases} \tag{B3}$$

[63] In the particular case in which the flow along the streamlines is purely advective (i.e., for $D_L = 0$), the solutions (B2) simplify as follows:

$$\begin{cases} C_1(\tau,t) &= C_{1,0}\exp\left(-K_{N(T)}\tau\right)H(t-\tau) \\ C_2(\tau,t)_{ox} &= C_{2,0}\exp\left(-K_{C(T)}\tau\right) \\ &\quad + C_{1,0}\dfrac{K_{N(T)}}{K_{C(T)}-K_{N(T)}}\left[\exp\left(-K_{N(T)}\tau\right)-\exp\left(-K_{C(T)}\right)\right]H(t-\tau), \\ C_4(\tau,t) &= C_{4,0} \\ C_3(\tau,t) &= 0 \end{cases} \tag{B4}$$

which coincide with the solution obtained by *Marzadri et al.* [2011] in the absence of local dispersion. On the other hand, along the anaerobic part of the streamlines, the concentration of the four Nr species assume the following expressions (obtained by solving the equations (A3), (A4) and (A8) with the respective boundary conditions):

$$\begin{cases} C_1(\tau,t) = C_{1,ox}(\tau_{\lim},\tau_{\lim}) \\ C_2(\tau,t)_{aox} = 0.5C_{2,ox}(\tau_{\lim},\tau_{\lim})C_{2,aox} \\ C_4(\tau,t) = 0.5C_{2,ox}(\tau_{\lim},\tau_{\lim})C_4 \\ C_3(\tau,t) = 0.5C_{2,ox}(\tau_{\lim},\tau_{\lim})C_3 \end{cases}, \tag{B5}$$

where

$$\begin{cases} C_{2,aox} = \exp\left[\dfrac{u^2\tau}{2D_L}\left[1+\sqrt{1+\dfrac{4K_{D(T)}D_L}{u^2}}\right]\right]erfc\left(\dfrac{u\tau+ut\sqrt{1+\frac{4K_{D(T)}D_L}{u^2}}}{2\sqrt{D_Lt}}\right) \\ \qquad + \exp\left[\dfrac{u^2\tau}{2D_L}\left(1-\sqrt{1+\dfrac{4K_{D(T)}D_L}{u^2}}\right)\right]erfc\left(\dfrac{u\tau-ut\sqrt{1+\frac{4K_{D(T)}D_L}{u^2}}}{2\sqrt{D_Lt}}\right) \\ C_4 = \exp\left(\dfrac{u^2\tau}{2D_L}\right)erfc\left(\dfrac{u\tau+ut}{2\sqrt{D_Lt}}\right)+erfc\left(\dfrac{u\tau-ut}{2\sqrt{D_Lt}}\right) \\ \qquad - \exp\left[\dfrac{u^2\tau}{2D_L}\left(1+\sqrt{1+\dfrac{4K_{D(T)N_{N_2O}}D_L}{u^2}}\right)\right]erfc\left(\dfrac{u\tau+ut\sqrt{1+\frac{4K_{D(T)N_{N_2O}}D_L}{u^2}}}{2\sqrt{D_Lt}}\right) \\ \qquad - \exp\left[\dfrac{u^2\tau}{2D_L}\left(1-\sqrt{1+\dfrac{4K_{D(T)N_{N_2O}}D_L}{u^2}}\right)\right]erfc\left(\dfrac{u\tau-ut\sqrt{1+\frac{4K_{D(T)N_{N_2O}}D_L}{u^2}}}{2\sqrt{D_Lt}}\right) \\ C_3 = \exp\left(\dfrac{u^2\tau}{2D_L}\right)erfc\left(\dfrac{u\tau+ut}{2\sqrt{D_Lt}}\right)+erfc\left(\dfrac{u\tau-ut}{2\sqrt{D_Lt}}\right) \\ \qquad - \exp\left[\dfrac{u^2\tau}{2D_L}\left(1+\sqrt{1+\dfrac{4K_{D(T)N_2}D_L}{u^2}}\right)\right]erfc\left(\dfrac{u\tau+ut\sqrt{1+\frac{4K_{D(T)N_2}D_L}{u^2}}}{2\sqrt{D_Lt}}\right) \\ \qquad - \exp\left[\dfrac{u^2\tau}{2D_L}\left(1-\sqrt{1+\dfrac{4K_{D(T)N_2}D_L}{u^2}}\right)\right]erfc\left(\dfrac{u\tau-ut\sqrt{1+\frac{4K_{D(T)N_2}D_L}{u^2}}}{2\sqrt{D_Lt}}\right). \end{cases} \tag{B6}$$

[64] Again for a purely advective transport ($D_L = 0$), the solutions (B5) become:

$$\begin{cases} C_1(\tau,t) &= C_{1,0}\exp\left(-K_{N(T)}\tau_{\lim}\right)H(t-\tau) \\ C_{2,aox}(\tau,t) &= C_{2,ox}\exp\left(-K_{C(T)}\tau\right) \\ &\quad + C_{1,0}\dfrac{K_{N(T)}}{K_{C(T)}-K_{N(T)}}\left[\exp\left(-K_{N(T)}\tau_{\lim}\right)\right. \\ &\quad \left. - \exp\left(-K_{C(T)}\tau_{\lim}\right)\right]\cdot H(t-\tau) \\ C_4(\tau,t) &= C_{2,aox}(\tau,t)_{aox}\left[1-\exp\left(K_{D(T)}\tau\right)\right]H(t-\tau) \\ C_3(\tau,t) &= C_{2,aox}(\tau,t)_{aox}\left[1-\exp\left(K_{D(T)}\tau\right)\right]H(t-\tau) \end{cases} \tag{B7}$$

which also coincide with the solutions obtained by *Marzadri et al.* [2011] in the absence of local dispersion.

## Notation

| | |
|---|---|
| $A_{dw}$ | downwelling area, $m^2$. |
| $A_{uw}$ | upwelling area, $m^2$. |
| $B$ | half width of channel, m. |
| $b_1$ | morphological parameter. |
| $b_2$ | morphological parameter. |
| $C_0$ | dissolved oxygen concentration, mg $l^{-1}$. |
| $C_{0,\lim}$ | dissolved oxygen concentration limit, mg $l^{-1}$. |
| $C_1$ | ammonium concentration, mg $l^{-1}$. |
| $C_2$ | nitrate concentration, mg $l^{-1}$. |
| $C_3$ | dinitrogen concentration, mg $l^{-1}$. |
| $C_4$ | nitrous oxide concentration, mg $l^{-1}$. |
| $C_{f,i}$ | concentration flux of the ith species, mg $l^{-1}$. |
| $C_i$ | resident concentration of the ith species, mg $l^{-1}$. |

$CV$ coefficient of variation.
$Cz$ dimensionless Chezy number.
$d_{50}$ mean grain size, m.
$Da$ Damkhöler dimensionless number.
$dA$ infinitesimal cross sectional area, $m^2$.
$D_L$ effective longitudinal dispersion coefficient, m $s^{-2}$.
$D_M$ molecular diffusion, $m^2$ $s^{-1}$.
$d_s$ relative submergence.
$f_0$ reaction rate for dissolved oxygen, mg $l^{-1}$ $s^{-1}$.
$f_1$ reaction rate for ammonium, mg $l^{-1}$ $s^{-1}$.
$f_2$ reaction rate for nitrate, mg $l^{-1}$ $s^{-1}$.
$f_3$ reaction rate for dinitrogen, mg $l^{-1}$ $s^{-1}$.
$f_4$ reaction rate for nitrous oxide, mg $l^{-1}$ $s^{-1}$.
$h$ hydraulic head, m.
$h_b$ head at the streambed, m.
$H_{BM}$ amplitude of alternate bars, m.
$K$ hydraulic conductivity, m $s^{-1}$.
$K_i$ rate coefficients at the hyporheic temperature T, $s^{-1}$.
$K_{i,(20C)}$ reaction rate coefficients at 20°C, $s^{-1}$.
$K_{RN}$ reaction rate of nitrification and respiration, $s^{-1}$.
$K1_{C(T)}$ half saturation (Monod) constant of biomass assimilation, mg $l^{-1}$.
$K1_{D(T)}$ half saturation (Monod) constant of denitrification, mg $l^{-1}$.
$K1_{N(T)}$ half saturation (Monod) constant of nitrification, mg $l^{-1}$.
$L$ bar wavelength, m.
$Nr_0$ total downwelling nitrogen mass flux, mg $l^{-1}$.
$P_i^{HZ}$ production of nitrogen gases.
$q$ water flux into the streambed surface, m $s^{-1}$.
$q_H$ hyporheic flow rate, m $s^{-1}$.
$Q_{M,dw}$ total mass flux of the ith species across the downwelling surface, mg $m^3$ $s^{-1}$ $l^{-1}$.
$Q_{M,up}$ total mass flux of the ith species across the upwelling surface, mg $m^3$ $s^{-1}$ $l^{-1}$.
$Q_S$ stream discharge, $m^3$ $s^{-1}$.
$RC$ relative concentration.
$R_i^{HZ}$ efficiency of hyporheic zone in removing the nitrogen species.
$R_i^S$ stream efficiency in removing nitrogen species.
$s$ distance measured along the streamline, m.
$s_0$ stream slope, m/m.
$T$ temperature, °C.
$t_f$ advective characteristics time scale, s.
$u$ longitudinal pore water Darcy velocity, m $s^{-1}$.
$v$ transverse pore water Darcy velocity, m $s^{-1}$.
$V$ stream velocity, m $s^{-1}$.
$w$ vertical pore water Darcy velocity, m $s^{-1}$.
$x$ longitudinal coordinate, m.
$y$ transversal coordinate, m.
$Y_0$ mean flow depth, m.
$Y_{BM}^*$ dimensionless depth.
$z$ vertical coordinate, m.
$z_d$ alluvium depth, m.
$\alpha_L$ longitudinal local dispersivity, m.
$\beta$ aspect ratio of alternate bars.
$\beta_b$ coefficient for experimental longitudinal dispersivity.
$\beta_c$ threshold value of the aspect ratio b for alternate bar formation.
$\varphi_i^{(T)}$ Arrhenius temperature coefficients for the ith species at temperature T.
$\eta(x, y)$ bed surface elevation, m.
$\mu_{C(T)}$ biomass assimilation potential maximum rate, $s^{-1}$.
$\mu_{D(T)}$ denitrification potential maximum rate, $s^{-1}$.
$\mu_{N(T)}$ nitrification potential maximum rate, $s^{-1}$.
$\mu_{\tau,up}$ mean of the travel time, s.
$\theta$ Shield number.
$\vartheta$ alluvium porosity.
$\sigma_{\tau,up}$ standard deviation of the travel time, s.
$\tau$ residence time, s.
$\tau^*_{up,50}$ dimensionless median hyporheic residence time.
$\tau_{\lim}$ residence time limit, s.
$\widetilde{\tau}$ dimensionless parameter for local redox condition at the streamline scale.
$\tau_{\tilde{H}Z}$ dimensionless parameter for local redox condition at any hyporheic control surface.
$\tau_{up,50}$ median hyporheic residence time, s.

[65] **Acknowledgments.** This research has been funded in part by the EU VII framework program through the project CLIMB (244151) and by the national program PRIN through the Analysis of Flow and Transport Processes at the Hillslope Scale project (2008A7EBA3).

## References

Alexander, R. B., R. A. Smith, and G. E. Schwarz (2000), Effect of stream channel on the delivery of nitrogen to the Gulf of Mexico, *Nature*, *403*, 758–761.

Arango, C. P., and J. L. Tank (2008), Land use influences the spatiotemporal controls of nitrification and denitrification in headwater streams, *J. N. Am. Benthol. Soc.*, *27*(1), 90–107.

Bailey, J. E., and D. F. Ollis (1977), *Biochemical Engineering Fundamentals*, McGraw Hill, New York.

Bear, J. (1972), *Dynamics of Fluid in Porous Media*, Dover, New York.

Beaulieu, J. J., C. P. Arango, S. K. Hamilton, and J. L. Tank (2008), The production and emission of nitrous oxide from headwater in the Midwestern United States, *Global Change Biol.*, *14*, 878–894.

Beaulieu, J. J., C. P. Arango, and J. L. Tank (2009), The effects of season and agriculture on nitrous oxide production in headwater streams, *J. Environ. Qual.*, *38*, 637–646.

Bellin, A., and Y. Rubin (2004), On the use of peak concentration arrival times for the influence of hydrogeological parameters, *Water Resour. Res.*, *40*, W07401, doi:10.1029/2003WR002179.

Binley, A. (2005), Groundwater–surface water interactions: A survey of UK field site infrastructure, *Sci. Rep. SC030155/SR5*, 49 pp., Environ. Agency, Bristol, U. K.

Boano, F., A. Demaria, R. Revelli, and L. Ridolfi (2010), Biochemical zonation due to intrameander hyporheic flow, *Water Resour. Res.*, *46*, W02511, doi:10.1029/2008WR007583.

Böhlke, J. K., and J. M. Denver (1995), Combined use of groundwater dating, chemical, and isotopic analyses to resolve the history and fate of nitrate contamination in two agricultural watersheds, Atlantic Coastal Plain, Maryland, *Water Resour. Res.*, *31*(9), 2319–2339.

Bottacin-Busolin, A., and A. Marion (2010), Combined role of advective pumping and mechanical dispersion on time scales of bed form–induced hyporheic exchange, *Water Resour. Res.*, *46*, W08518, doi:10.1029/2009WR008892.

Buffington, J. M., and D. Tonina (2009), Hyporheic exchange in mountain rivers II: Effects of channel morphology on mechanics, scales, and rates of exchange, *Geogr. Compass*, *3*(3), 1038–1062.

Buss, S. R., M. O. Rivett, P. Morgan, and C. D. Bemment (2006), Attenuation of nitrate in the sub-surface environment, *Sci. Rep. SC030155/SR2*, Environ. Agency, Bristol, U. K.

Cardenas, M. B., P. L. M. Cook, H. Jiang, and P. Traykovski (2008), Constraining denitrification in permeable wave-influenced marine sediment using linked hydrodynamic and biogeochemical modeling, *Earth Planet. Sci. Lett.*, *275*, 127–137.

Colombini, M., G. Seminara, and M. Tubino (1987), Finite-amplitude alternate bars, *J. Fluid Mech.*, *181*, 213–232.

Cvetkovic, V., and G. Dagan (1994), Transport of kinetically sorbing solute by steady random velocity in heterogeneous porous formation, *J. Fluid Mech.*, *265*, 189–215.

Dagan, G., V. Cvetkovic, and A. M. Shapiro (1992), A solute flux approach to transport in heterogeneous formations: 1. The general framework, *Water Resour. Res.*, *28*(5), 1369–1376, doi:10.1029/91WR03086.

Dent, C. L., and J. C. Henry (1999), Modelling nutrient–periphyton dynamics in streams with surface–subsurface exchange, *Ecol. Modell.*, *122*, 97–116.

Duff, J. H., and F. Triska (2000), Nitrogen biogeochemistry and surface-subsurface exchange in streams, in *Streams and Groundwaters*, edited by J. Jones and P. Muholland, pp. 197–220, Academic, Boston.

Elliott, A. H., and N. H. Brooks (1997), Transfer of nonsorbing solutes to a streambed with bed forms: Theory, *Water Resour. Res.*, *33*(1), 123–136, doi:10.1029/96WR02784.

Fernald, A. G., D. H. Landers, and P. J. Wigington Jr. (2006), Water quality changes in hyporheic flow paths between a large gravel bed river and off-channel alcoves in Oregon, USA, *River Res. Appl.*, *22*, 1111–1124.

Fogler, H. S. (1999), *Elements of Chemical Reaction Engineering*, Prentice Hall, Englewood Cliffs, N. J.

Galloway, J. N., J. D. Aber, J. W. Erisman, S. P. Seitzinger, R. W. Howarth, E. B. Cowling, and B. J. Cosby (2003), The nitrogen cascade, *BioScience*, *53*(4), 341–356.

Gelhar, L. W., and M. A. Collins (1971), General analysis of longitudinal dispersion in nonuniform flow, *Water Resour. Res.*, *7*(6), 1511–1521, doi:10.1029/WR007i006p01511.

Gooseff, M. N. (2010), Defining hyporheic zones- advancing our conceptual and operational definitions of where stream water and groundwater meet, *Geogr. Compass*, *4*(8), 945–955.

Kelso, B., R. Smith, and R. Laughlin (1999), Effects of carbon substrate on nitrite accumulation in freshwater sediments, *Appl. Environ. Microbiol.*, *65*, 61–66.

Kendall, C., E. M. Elliott, and S. D. Wankel (2007), Tracing anthropogenic inputs of nitrogen to ecosystems, in *Stable Isotopes in Ecology and Environmental Science*, 2nd ed., edited by R. H. Michener and K. Lajtha, pp. 375–449, Blackwell Sci., Oxford, U. K.

Kjellin, J., S. Hallin, and A. Wörman (2007), Spatial variations in denitrification activity in wetland sediments explained by hydrology and denitrifying community structure, *Water Res.*, *41*(20), 4710–4720.

Krause, S., L. Heathwaite, A. Binley, and P. Keenan (2009), Nitrate concentration changes at the groundwater–surface water interface of a small Cumbrian river, *Hydrol. Processes*, *23*(15), 2195–2211.

Maier, R. M. M., J. L. Pepper, and C. P. Gerba (2009), *Environmental Microbiology*, Academic, London.

Marion, A., M. Bellinello, I. Guymer, and A. I. Packman (2002), Effect of bed form geometry on the penetration of nonreactive solutes into a streambed, *Water Resour. Res.*, *38*(10), 1209, doi:10.1029/2001WR000264.

Marzadri, A., D. Tonina, A. Bellin, G. Vignoli, and M. Tubino (2010), Semianalytical analysis of hyporheic flow induced by alternate bars, *Water Resour. Res.*, *46*, W07531, doi:10.1029/2009WR008285.

Marzadri, A., D. Tonina, and A. Bellin (2011), A semianalytical three-dimensional process-based model for hyporheic nitrogen dynamics in gravel bed rivers, *Water Resour. Res.*, *47*, W11518, doi:10.1029/2011WR010583.

Master, Y., U. Shavit, and A. Shaviv (2005), Modified isotope pairing technique to study N transformations in polluted aquatic systems: Theory, *Environ. Sci. Technol.*, *39*, 1749–1756.

McLaren, A. D. (1976), Rate constants for nitrification and denitrification in soils, *Rad. Environ. Biophys*, *13*, 43–48.

Mulholland, P. J., H. M. Valett, J. R. Webster, S. A. Thomas, L. W. Cooper, S. K. Hamilton, and B. J. Peterson (2004), Stream denitrification and total nitrate uptake rates measured using a field $^{15}$N tracer addition approach, *Limnol. Oceanogr.*, *49*(3), 809–820.

Mulholland, P. J., et al. (2008), Stream denitrification across biomes and its response to anthropogenic nitrate loading, *Nature*, *452*, 202–206.

Naiman, R. J., and R. E. Bilby (1998), *River Ecology and Management: Lessons From the Pacific Coastal Ecoregion*, Springer, New York.

Peterson, B., et al. (2001), Control of nitrogen export from watershed by headwater streams, *Science*, *292*, 86–89.

Pfankuch, H. O. (1963), Contribution à l'étude des déplacements de fluides miscibles dans un milieu poreux, *Rev. Inst. Fr. Petrol.*, *18*(2), 215–270.

Pinay, G., T. C. O'Keefe, R. T. Edwards, and R. J. Naiman (2009), Nitrate removal in the hyporheic zone of a salmon river in Alaska, *River Res. Appl.*, *25*(4), 367–375.

Puckett, L. J., C. Z. H. Essaid, J. T. Wilson, H. M. Johnson, M. J. Brayton, and J. R. Vogel (2008), Transport and fate of nitrate at the ground-water/surface-water interface, *J. Environ. Qual.*, *37*, 1034–1050.

Rutherford, J. C. (1994), *River Mixing*, John Wiley, Chichester, U. K.

Saffman, P. G. (1960), On the effect of the molecular diffusivity in turbulent diffusion, *J. Fluid Mech.*, *8*, 263–273.

Sawyer, A. H., M. B. Cardenas, and J. Buttles (2011), Hyporheic exchange due to channel-spanning logs, *Water Resour. Res.*, *47*, W08502, doi:10.1029/2011WR010484.

Shapiro, A. M., and V. Cvetkovic (1988), Stochastic analysis of solute arrival time in heterogeneous porous media, *Water Resour. Res.*, *24*(10), 1711–1718, doi:10.1029/WR024i010p01711.

Sheibley, R. V., A. P. Jackman, J. H. Duff, and F. J. Triska (2003), Numerical modeling of coupled nitrification–denitrification in sediment perfusion cores from the hyporheic zone of the Shingobee River, MN, *Adv. Water Resour.*, *26*, 977–987.

Sjodin, A. L., W. M. Lewis Jr., and J. F. Saunders III (1997), Denitrification as a component of the nitrogen budget for a large plains river, *Biogeochemistry*, *39*, 327–342.

Spalding, R. F., and M. E. Exner (1993), Occurrence of nitrate in groundwater—A review, *J. Environ. Qual.*, *22*(3), 392–402.

Sylvia, D. M., J. J. Fuhrmann, P. G. Hartel, and D. A. Zuberer (2005), *Principles and Applications of Soil Microbiology*, 550 pp., Prentice Hall, Upper Saddle River, N. J.

Tonina, D., and J. M. Buffington (2007), Hyporheic exchange in gravel bed rivers with pool-riffle morphology: Laboratory experiments and three-dimensional modeling, *Water Resour. Res.*, *43*, W01421, doi:10.1029/2005WR004328.

Tonina, D., and J. M. Buffington (2009a), Hyporheic exchange in mountain rivers I: Mechanics and environmental effects, *Geogr. Compass*, *3*(3), 1063–1086.

Tonina, D., and J. M. Buffington (2009b), A three-dimensional model for analyzing the effects of salmon redds on hyporheic exchange and egg pocket habitat, *Can. J. Fish. Aquat. Sci.*, *66*, 2157–2173, doi:10.1139/F09–146.

Tonina, D., and J. M. Buffington (2011), Effects of stream discharge, alluvial depth and bar amplitude on hyporheic flow in pool-riffle channels, *Water Resour. Res.*, *47*, W08508, doi:10.1029/2010WR009140.

Triska, F. K., J. H. Duff, and R. J. Avanzino (1993), The role of water exchange between a stream channel and its hyporheic zone in nitrogen cycling at the terrestrial-aquatic interface, *Hydrobiologia*, *251*, 167–184.

Valett, M., J. Morrice, C. Dahm, and M. Campana (1996), Parent lithology, surface-groundwater exchange, and nitrate retention in headwater streams, *Limnol. Oceanogr.*, *41*(2), 333–345.

van Genuchten, M. T., and W. J. Alves (1982), Analytical solutions of the one-dimensional convective-dispersive solute transport equation, *Tech. Bull. 1661*, 151 pp., U. S. Dep. of Agric., Washington, D. C.

Zarnetske, J. P., R. Haggerty, S. M. Wondzell, and M. A. Baker (2011), Dynamics of nitrate production and removal as a function of residence time in the hyporheic zone, *J. Geophys. Res.*, *116*, G01025, doi:10.1029/2010JG001356.